Joint International Topical Meeting on Mathematics & Computation and Supercomputing in Nuclear Applications (M&C + SNA 2007)
Monterey, California, April 15-19, 2007, on CD-ROM, American Nuclear Society, LaGrange Park, IL (2007)

LARGE EDDY SIMULATION OF WIRE-WRAPPED FUEL PINS I: Hydrodynamics of a Single Pin

Paul Fischer, James Lottes, and Andrew Siegel
Mathematics and Computer Science Division
Argonne National Laboratory
Argonne, IL 60439
fischer@mcs.anl.gov, jlottes@mcs.anl.gov, siegela@mcs.anl.gov

Giuseppe Palmiotti
Nuclear Engineering Division
Argonne National Laboratory
Argonne, IL 60439
GPalmiotti@anl.gov

ABSTRACT

We present large-eddy simulations of flow and heat transfer in a wire-wrapped fuel assembly at subchannel Reynolds numbers of Re_h=4684–29184. The domain consists of a single pin in a hexagonally periodic array, corresponding to two interior subchannels. Periodic boundary conditions are also used in the axial direction over a single wire-wrap period.

Key Words: wire-wrapped fuel pin

1. Introduction

Proposed designs for advanced burner reactors call for liquid sodium coolant passing through subassemblies of hexagonally arrayed fuel pins. The fuel pins in each subassembly are separated by wire wrap spacers wound helically along the pin axes. A single assembly will comprise 217 pins in a hexagonal array, with about 5 turns of the wire along the length of each pin. In addition to spacing the pins, the wire wrap is designed to promote mixing of the coolant between the channels that are formed by the pin array. Enhanced mixing can lead to reduced peak pin temperatures. The ability to predict (and optimize) mixing behavior can lead to reduced hot channel factors and thereby allow operation at higher power levels. In addition to the mixing, it is of interest in the design of the overall core to predict the distribution of the coolant flow, including the amount passing through the near-wall subchannels.

Analysis of wire-wrapped fuel pins is challenging for several reasons. The Reynolds number based on the hydraulic radius, $Re_h = UD_h/\nu$, is in the range of 40000–65000, which means the flow is turbulent. The turbulence is further promoted by the wire wrap. Because it creates multiple contact points and lines, the wire wrap makes the geometry (and mesh) relatively complex. Moreover, with > 400 subchannels and $L/D_h \approx 360$, the geometry of just a single subassembly is large. There are hundreds of assemblies in the reactor. Most thermal-hydraulics analysis is therefore based on subchannel modeling, which use a few hundred degrees of freedom per channel to represent mass, momentum, and energy balances at axial positions along the channel. Subchannel models of a full core will have $\sim 10^7$ control volumes. Subchannel models are relatively fast and will likely be the mainstay of reactor-scale analysis for the foreseeable future. However, they rely on experimentally determined coefficients to account for interchannel mixing.

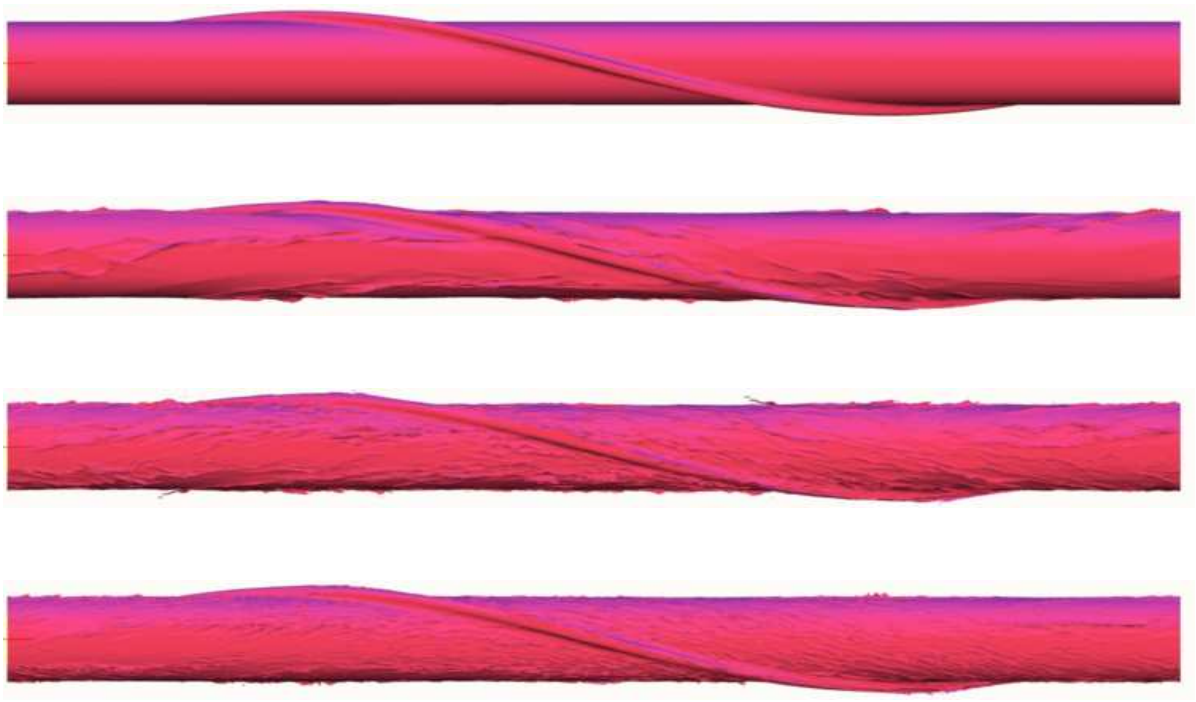

Figure 1. Isosurfaces of axial velocity ($w = 0.5U_0$) at startup for $H/D = 13.4$, Re_h=4684: (top to bottom) tU/D=.05, 5.05, 10.05, 15.05. Flow is from left to right.

Computational fluid dynamics (CFD) offers the opportunity for detailed analyses that may lead to improvements in the subchannel model coefficients and may also provide a means of validating the applicability of subchannel models to specific (albeit reduced) geometries a posteriori. Several efforts to apply CFD to wire-wrap geometries are already underway, including the recent work of Ahmad and Kim [1], who use CFD coupled with a turbulence model based on the Reynolds averaged Navier-Stokes (RANS) equations to study 7- and 19-pin configurations. These results are encouraging and it appears that RANS computations can provide the detailed flow analysis that will be required for improved modeling insight and that will be important for coupling to equally detailed neutronics computations. A particular challenge for RANS models, which also require empirical constants, is to properly identify separation zones in regions of adverse pressure gradient (e.g., on the leeward side of the wire).

At a finer scale, one can also consider CFD based on direct numerical or large eddy simulation (DNS or LES), in which the governing equations are solved with either no (DNS) or minimal (LES) closure modeling. In the case of LES, one simulates only the energy-carrying large scales of motion and typically augments the Navier-Stokes equations with a spatially varying dissipation mechanism such as an eddy- or hyperviscosity to account for subgrid scale motion.

2 Filtered Spectral Element Simulations

As an initial step towards parameter-free thermal-hydraulic simulation, we have analyzed a single periodic cell in the wire-wrap geometry of Fig. 1 using the spectral element method (SEM) introduced by Patera

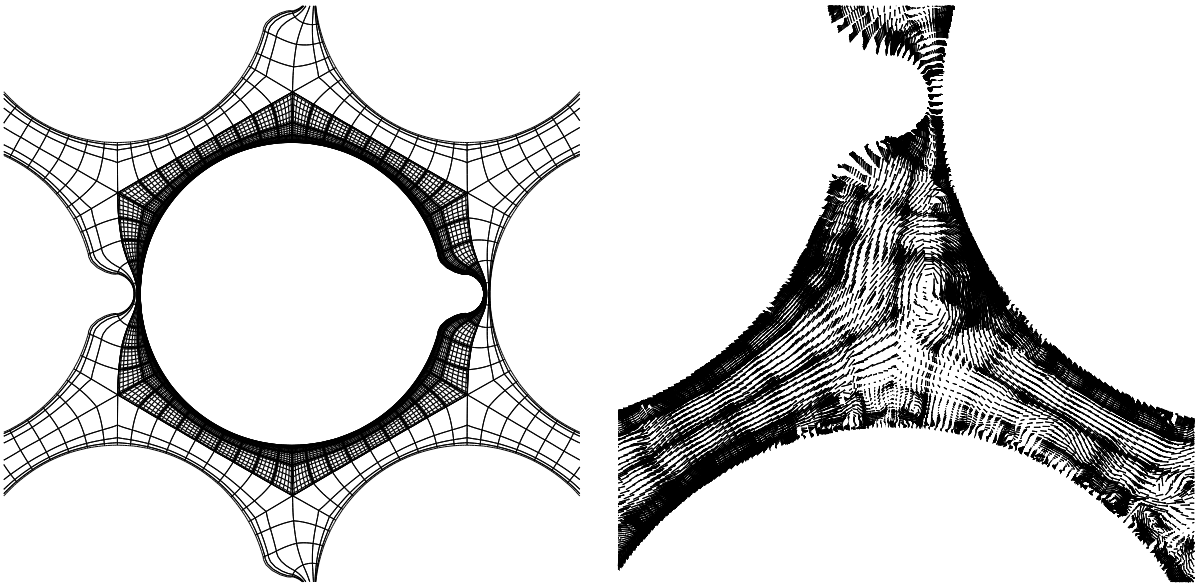

Figure 2. Cross-section of comptational mesh at z=0: (left) tiled mesh showing computational domain highlighted with the nodal distribution for N=7; (right) close up of instantaneous in-plane velocity at z=0 for H/D=13.4, $Re = 28104$, $N = 9$.

in 1984 [8]. The SEM is a high-order weighted residual technique that combines the geometric flexibility of finite elements with the rapid convergence and tensor-product efficiencies of global spectral methods. Within each of E elements, the solution, data, and geometry are approximated by Nth-order tensor-product polynomials, resulting in $n \approx EN^3$ grid points. The polynomials are Lagrangian interpolants based on the Gauss-Lobatto-Legendre quadrature points, which provide for stable and efficient evaluation of the bilinear forms arising in the weighted residual formulation. Because it has minimal numerical dissipation and dispersion, the SEM is ideally suited for high fidelity transport of small scale structures, as arise in the present case [3].

The current simulations are based on the $\mathbb{P}_N - \mathbb{P}_{N-2}$ formulation of Maday and Patera [7], which uses a discontinuous pressure approximation of order $N-2$ and continuous velocity approximations of order N. Time advancement is semi-implicit, with explicit treatment of the nonlinear terms and implicit treatment of the viscous and pressure/incompressiblity terms. The latter are further decoupled through an algebraic splitting that leads to discrete Helmholtz solves for the velocity components and a discrete Poisson equation for the pressure, each of which is solved using preconditioned conjugate gradient iteration. Preconditioning for the pressure system is based on the spectral element multigrid procedure developed in [4].

The time advancement is augmented with the stabilizing filter developed in [5], which removes energy from the highest modes and thus serves as a drain for the energy cascade. Because it damps only the highest order modes within each element, the filter retains spectral accuracy and automatically shuts off in regions where the flow is well resolved. The filter thus acts like a hyperviscosity and has been successfully used in a prior study of rod bundles in a square lattice [6].

The pin geometry corresponds to the configuration of Cheng and Todreas [2] with a pitch to diameter ratio of $P/D = 1.154$ and helical wire-wrap pitch of $H = 13.4\,D$. The hydraulic diameter in this case is $D_h = .4684D$, not accounting for the presence of the wire. The wire diameter, D_w, is 90.6% of the

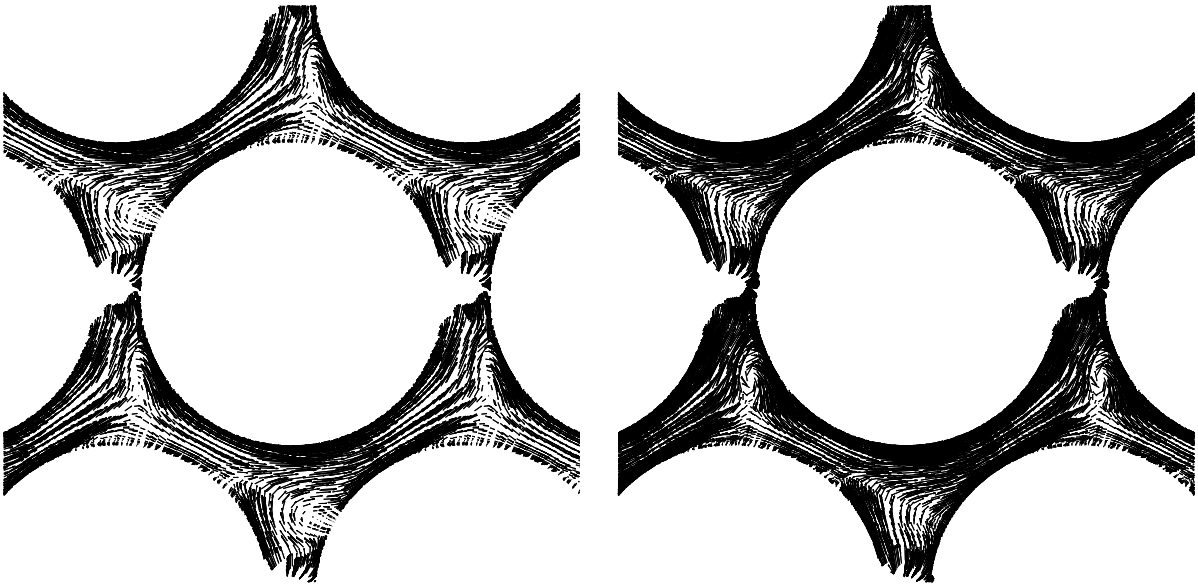

Figure 3. Mean velocity distributions at $z = 0$ for (left) $Re = 14052$, H/D=20.1, N=7 and (right) $Re = 28104$, H/D=13.4, N=9. Only 1/4 of the vectors are shown.

minimum gap and a fillet of radius $.6D_w$ is added to simplify the meshing. Both axial and horizontal periodicity were assumed, corresponding to a pin located in the middle of the assembly, as illustrated in Fig. 2. (Seven-pin configurations comprising 18 subchannels are currently under investigation.) Our single-pin (two-subchannel) geometry is discretized with E=29520 elements of order N=7 (8.7 M points), which provides roughly 28 points across each subchannel half-width and 840 points in the axial direction. Simulation of one flow-through time requires 15 hours on 2048 processors of the IBM BlueGene at Argonne. For H/D=13.4, we studied Reynolds numbers Re_h=4684, 14592, and 29184, using N=9 in the latter case. We also examined the case of H/D=20.1, Re_h=14592, using N=7. Statistics were typically gathered over a single flow-through time.

Flow through the domain was imposed by applying a body force in the z direction, corresponding to a mean axial pressure drop. Because of the linearity of the implicit substeps, it is possible to implicitly establish the forcing necessary to maintain a constant mean flow velocity U by first advancing the Navier-Stokes system without a body force and then adding to the resultant velocity/pressure fields an auxiliary solution, $(\alpha \mathbf{u}_0, \alpha p_0)$. The constant α is chosen at each step such that the net solution satisfies the desired flow rate. The fields $(\mathbf{u}_0, p_0)$ solve the unsteady Stokes problem with unit forcing and are precomputed once and stored.

3 Results

Figure 2 (right) shows a typical in-plane velocity field for Re=28104, N=9 at z=0. The small-scale structures oscillate rapidly and tend to move with the passage of the low-speed streaks (Fig. 1). The large vortex near the center, however, is relatively persistent at this axial station and is a result of separation from the wire below. This central vortex is evident in the time-averaged velocity distributions of Fig. 3 and was also observed in the RANS calculations of Ahmad and Kim [1]. The vortex at the 6 o'clock position in the Re=14052 case of of Fig. 3 (left) appears to subside with increased Reynolds number (right) and was not present in the $Re = 60840$ RANS computation [1].

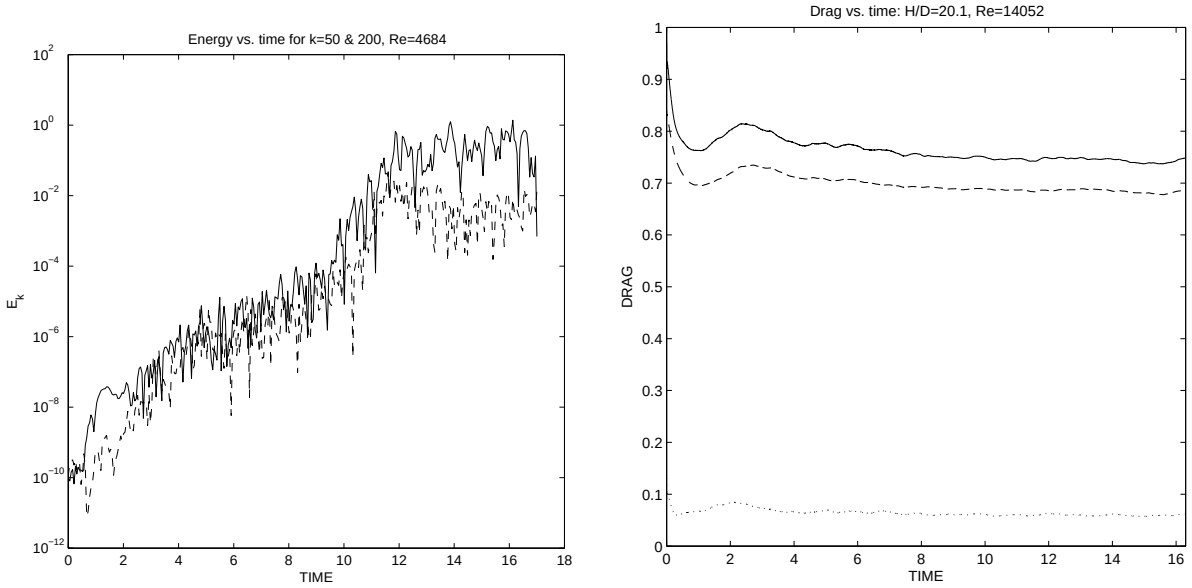

Figure 4. (left) Evolution of kinetic energy at wavenumbers $k = 50$ (solid) and $k = 200$ (dashed) taken along the subchannel centerline for $Re = 4684$, H/D=13.4; (right) evolution of drag, normalized by ρU^2, for $Re = 14052$, H/D=20.1.

The flow typically reached a saturated nonlinear state within one flow-through time, indicating that turbulence will saturate within the first wire pitch in the developing (i.e., non-periodic) flow case. This observation is consistent with experimental observations that development lengths are typically less than H. The evolution to turbulence is evident in Fig. 1, which shows the development of low-speed streaks near the pin surface at times tU/D=.05–15.05. Figure 4 (left) shows the kinetic energy history, $E_k(t)$, for wave numbers $k = 50$ and 200, for impulsively started flow. It is clear that even the high wave number energy saturates by $t/UD \approx 12$, well within a single flow-through time. Here, $E_k(t)$ is computed from the Fourier transform of the axial distribution of the velocity along one of the channel centerlines at several time instances. Figure 4 (right) shows the evolution of the total drag, skin friction, and form drag, normalized by ρU^2 for the Re_h=14592, H/D=20.1 case, which was started from H/D=13.4 solution. Form drag accounts for about 8% of the net pressure drop for these configurations.

The typical flow pattern is evident from the distribution of low-speed streaks in the bottom panel of Fig. 1. The flow wraps around the pin on the leeward side of the wire and is thus drawn into a subchannel after the wire crosses into the subchannel. This point is further illustrated in Fig. 5, which shows the velocity distributions at the subchannel boundaries marked A, B, C in the top right figure. In the left figure, the three interfaces have been shifted to be in phase. The flow in the lower half of each panel is into the channel, following the wire. Instantaneous and mean distributions are shown. The three mean distributions have been averaged in the last column, and this data was then integrated in the wall-normal direction to compute the mean interchannel velocity, which is shown lower-right. (The curve has been periodically extended for purposes of illustration.) Also shown as dotted curves are sinusoidal approximations given by $a\sin(2\pi z/H + \phi)$, with $phi = 0.43$ and a=.290 for H=13.4 and a=.225 for H=20.1. Note that peak amplitudes of the ratio of cross-flow to axial-flow velocities exceeds the slopes of the wire (e.g., $\Delta x/\Delta z$), which are 0.27 and 0.18, respectively, for H=13.4 and 20.1.

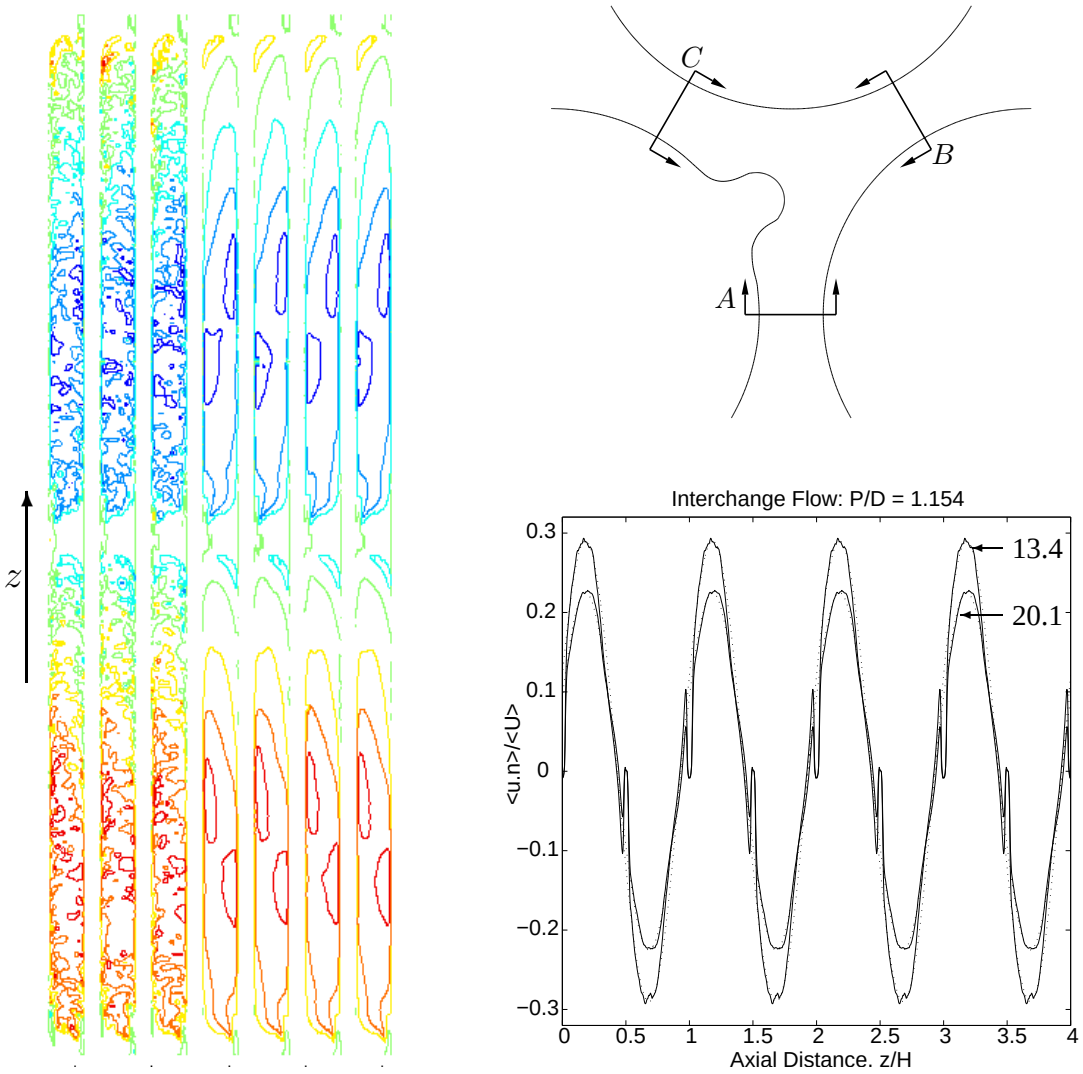

Figure 5. Interchannel velocity distributions for H/D=20.1: (left, cols. 1–3) instantaneous distributions at A, B, C with expanded horizontal scale and B and C sections shifted in z to match A; (cols. 4–6) mean distributions at A, B, C; (col. 7) average of three mean distributions; (right, top) subchannel geometry; (right, bottom) time- and spanwise-averaged velocity along channel interfaces for H/D=20.1 (lower curve) and 13.4 (upper curve). Dotted lines correspond to $a\sin(2\pi z/H+\phi)$ with ϕ=0.43 and a=.290 (H=13.4) and a=.225 (H=20.1).

4 Summary

We have made a preliminary investigation of the hydrodynamics of wire-wrapped fuel pins. While these results do not yet address important features such as wall and corner channels, they do serve as a starting point for insight into interchannel transport. The simulations also provide accurate flow fields that can be directly coupled with larger (i.e., multichannel) thermal hydraulics computations or used to provide accurate mean and fluctuating flow fields that can serve as surrogate flow fields. We anticipate expanding this work to include multiple channels, including wall and corner channels, in the near future.

Acknowledgments

This work was supported by the U.S. Dept. of Energy under Contract DE-AC02-06CH11357.

REFERENCES

[1] A. Ahmad and K.-Y. Kim, *Three-dimensional analysis of flow and heat transfer in a wire-wrapped fuel assembly*, Proc. of ICAPP 05 (Seoul, Korea), 2005.

[2] S.K. Cheng and N.E. Todreas, *Models and correlations for bare and wire-wrapped hexagonal rod bundles- bundle friction factors, subchannel friction factors and mixing parameters*, Nuclear Eng. and Design.

[3] P.F. Fischer, G.W. Kruse, and F. Loth, *Spectral element methods for transitional flows in complex geometries*, J. Sci. Comput. **17** (2002), 81–98.

[4] P.F. Fischer and J.W. Lottes, *Hybrid Schwarz-multigrid methods for the spectral element method: Extensions to Navier-Stokes*, Domain Decomposition Methods in Science and Engineering Series (R. Kornhuber, R. Hoppe, J. Priaux, O. Pironneau, O. Widlund, and J. Xu, eds.), Springer, Berlin, 2004.

[5] P.F. Fischer and J.S. Mullen, *Filter-based stabilization of spectral element methods*, Comptes rendus de l'Académie des sciences, Série I- Analyse numérique **332** (2001), 265–270.

[6] P.F. Fischer and C.P. Tzanos, *Filtered simulations of turbulence in a reactor rod bundle flow*, Proc. Am. Nuc. Soc. Mtg., San Diego, June 2005. Preprint ANL/MCS-P1213-0105 (2005).

[7] Y. Maday and A.T. Patera, *Spectral element methods for the Navier-Stokes equations*, State-of-the-Art Surveys in Computational Mechanics (A.K. Noor and J.T. Oden, eds.), ASME, New York, 1989, pp. 71–143.

[8] A.T. Patera, *A spectral element method for fluid dynamics : laminar flow in a channel expansion*, J. Comput. Phys. **54** (1984), 468–488.